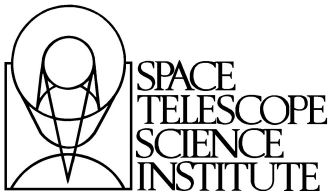


**Instrument Science Report WFC3 2014-21**

# Infrared Blobs: Time-dependent Flags

P. R. McCullough, J. Mack, M. Dulude, and B. Hilbert

*Updated* March 30, 2018

**ABSTRACT**

*We describe the creation of time-dependent flags for pixels associated with "blobs" on the WFC3 IR detector. We detect the blobs on flat fields obtained by repeated observations of the night side of the Earth. We provide the most complete census of IR blobs' positions, radii, and times of first appearance. In aggregate, a set of 46 blobs, 27 "strong" and 19 "medium" in their effective scattering cross section, affect slightly less than 1% of the pixels of the detector. A second set of 81 "weak" (and typically smaller) blobs affect another 1% of the pixels. In the past, the "blob" flag, bit 9 (i.e. value = 512) in the data quality (DQ) array described in Table 2.5 of the WFC3 Data Handbook (Rajan et al. 2010) has been a static 2-D array; henceforth a set of such arrays, each associated with a "use after" date corresponding to the appearance of one or more new blobs, can be used. We prepared such DQ arrays using the 46 "strong" and "medium" blobs and discuss why we did not include the fainter blobs therein. As an added data product, we create and test a blob flat field that corrects the effects of blobs on extended emission; however, it should <u>not</u> be applied if stellar photometry is the goal.*

***keywords**: Hubble Space Telescope, HST - instrumentation: detectors - methods: data analysis - techniques: image processing - Wide Field Camera 3, WFC3*

## Introduction

As noted by Pirzkal & Hilbert (2012) and Pirzkal, Viana, & Rajan (2010), blobs are defocused images of particulates on the channel select mechanism (CSM) corresponding to regions of slightly lower than nominal sensitivity. New blobs appear occasionally throughout the mission as the CSM mirror accumulates particulates. In order to flag pixels associated with the blobs appropriately, we need a list of blob positions, radii, and

times of first appearance. The CALWF3 pipeline can apply the latter via a reference file, specifically the bad pixel table (BPIXTAB), in a "use after" manner in order to flag the pixels associated with a given blob only after its appearance and not before.

## Observations

We used ~100 flat fields obtained between 2013-07-30 and 2014-03-22 under program 13499 (McCullough P.I.) to generate a "grand average" image of the detector in the filter F153M. We used all dark-Earth flat fields from July 2010 to the present (programs 11917, 12709, 13068, 13182, 13099, 13499, 13588) to determine the first appearance of each blob if not already noted in Table 1 of Pirzkal & Hilbert (2012).

## Identifying and Characterizing Blobs

To identify blobs, we began with a "grand average" image, specifically the median of ~100 dark-Earth F153M uncalibrated ("raw") images divided by a median of a much smaller set of F153M internal flat fields. Ideally, the "grand average" image would be unity everywhere, but in so far as it is not, it represents deviations of the external flat from the internal flat and, of course, Poisson noise and detector noise, both averaged down considerably. We subtracted the "grand average" image values from unity, so that the blobs are positive deviations, i.e. so they would look like stars (or galaxies) above a background of zero. We clamped all pixels values greater than 0.2 to be 0.2 and all less than -0.2 to be -0.2; this reduces the influence of clusters of "wild" pixels, especially near the edges and corners. We median filtered the result with a 3x3 pixel kernel to remove individual deviant pixels. We multiplied the resulting image by 1000 in order for a particular star-finding algorithm (IDL's version of *DAOfind*) to work well. Figure 1 shows the resulting image of blobs.

The parameters for IDL's *DAOfind.pro* that worked well in finding blobs even in the presence of their ~3x variation in radius across the detector were as follows: S/N threshold *hmin* = 4, *roundness* -0.5 to 1.0, *sharpness* -1.0 to 1.0, and *FWHM* = 15 pixels. Only the *FWHM* was critical; it needed to be large enough that the *DAOfind* algorithm would detect the defocused blobs and estimate their centers accurately. (Using a much smaller FWHM caused the algorithm to detect a number of blobs around the periphery of each large-diameter blob). From the large number of blobs reported, we defined limits of integrated flux F for three categories: weak ($13.1 < F < 26.2$), medium ($26.2 < F < 52.4$), and strong blobs ($F > 52.4$). (The units are parts per thousand, because we had multiplied the normalized flat field by 1000. For example, 52.4 corresponds to a diminution of light by 5.2%.). In Figure 1 and Table 1, the blobs are identified in the three categories by blue, green, and red circles, respectively. In addition, there are five blobs that we identified and added by hand; these five "cyan" blobs have large radii and low surface

brightness; apparently, the “cyan” blobs are marginally weaker than the “blue” (weak) blobs.

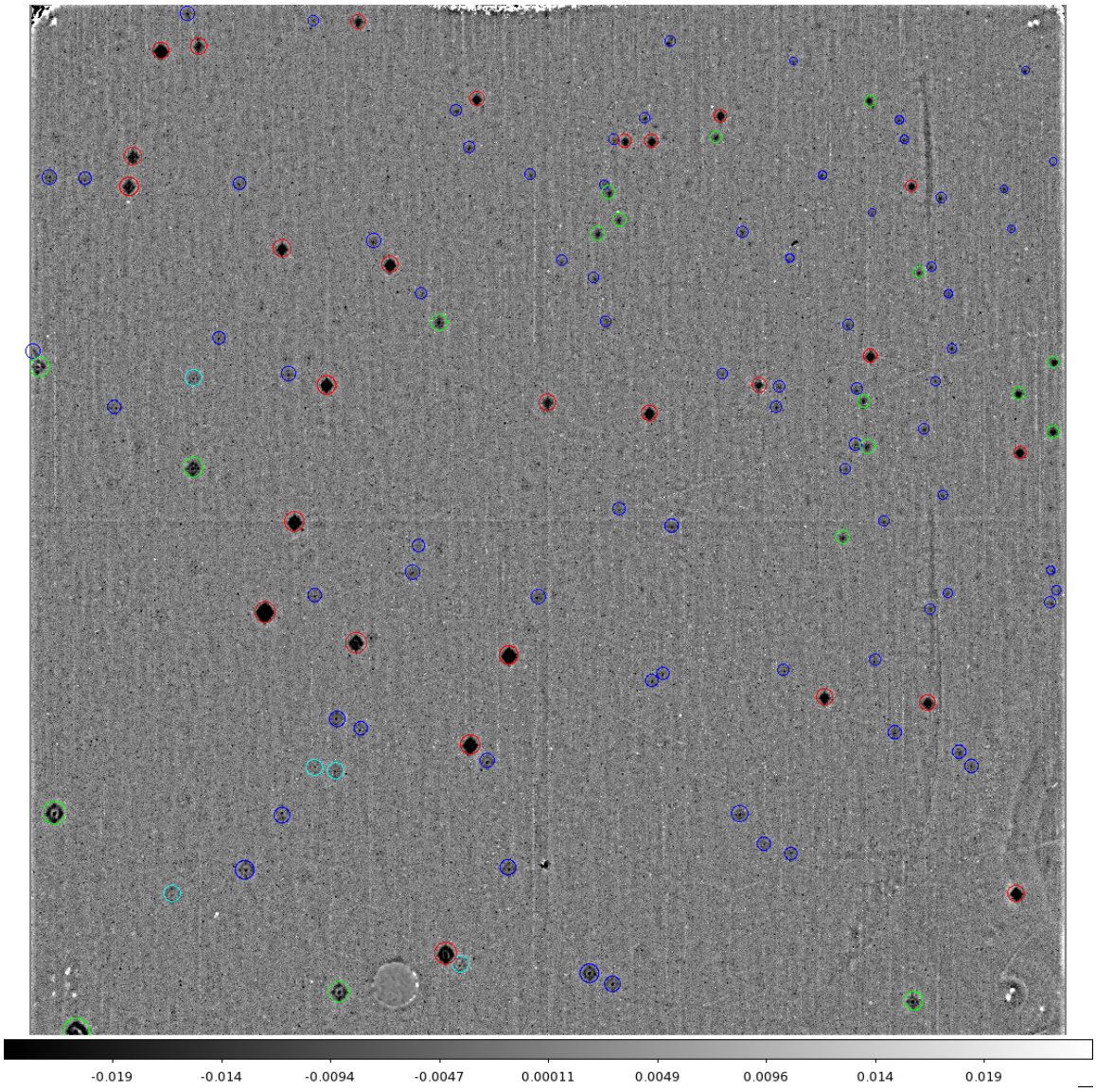


**Figure 1: Blobs on the WFC3 IR detector. Strong (red), medium (green) and weak (blue) blobs are indicated by circles. Only the strong and medium blobs (red and green circles) are flagged in the published BPIXTABs. The radii increase from the upper right corner to the lower left corner. Four weak, large-radii blobs (cyan) were added by hand after visual inspection; the automatic algorithm did not find them, or if it did, their estimated flux was below the threshold selected. A few dozen blobs identified by the algorithm were rejected by visual inspection and are not shown; most of them were associated with defects near the detector’s corners, the “death star” circle in the lower left quadrant, and other unrelated features of the flat field. (The centering of the circles on the blobs is more accurate than indicated by this ds9 display.)**

The blobs’ radii vary systematically across the detector; they are nearly in focus in the upper right corner and they become increasingly defocused toward the lower left corner. We estimated the radius R (in pixels) for each blob by an empirical formula:

$$R = (13 - 0.006\,L)\sqrt{F/32}, \qquad F < 32$$
$$= (13 - 0.006\,L) \qquad F > 32,$$

where L is the projected distance (in pixels) of the blob at detector position (X,Y) along the diagonal connecting the lower left corner to the upper right corner of the detector,

$$L = \cos(45°)\ X + \sin(45°)\ Y.$$

For examples, at (X, Y) = (0, 0), L = 0 pixels and R = 13.0 pixels; at (X, Y) = (512, 512) or (1024, 0) or (0, 1024), L = 724 pixels and R = 8.66 pixels; at (X, Y) = (1024, 1024), L = 1448 pixels and R = 4.3 pixels. The values of R are such that a circle of that radius centered on the blob will enclose all of the pixels affected by the blob, as determined empirically by visual inspection of the "grand average" image with appropriate circles superposed.

## Creating the "useafter" bpx.fits Files

If not available from Table 1 of Pirzkal (2012), we determined the first appearance of each blob by visual inspection of a grid of cutouts centered on each blob. An example is shown in Figure 2. The resulting dates of "first appearance" are given in the last column of Table 1. Actually, the date reported is not the date we first saw the blob in the dark-Earth images, but more exactly the latest date that we did not see it in those images. The latter choice guarantees that the blob's pixels will be flagged in all science images in which the given blob could appear.

We have generated a new set of bad pixel files for the IR channel which capture the timing of the blobs' appearances, i.e. which contain only the blobs present on the detector on a given date. The blobs have been flagged with a value of 512 ("bad in flat") in the BPIXTAB. Other common "bad" flag values include bad detector pixels (4), unstable in zero-read (8), unstable response (32), and bad reference pixel (128) all of which have been computed from in-flight darks and internal flats (Table E.2 in the WFC3 Instrument Handbook).

Prior to this work, there were two sets of these "other" bad pixel tables corresponding to two unique useafter dates: the first (u4c1709ri_bpx.fits) has a useafter date of the launch date, 14 May 2009 (MJD 54965) and the second (w681807ii_bpx.fits) has a useafter date of 13 Jun 2010 (MJD 55360) and contains a much larger population of deviant pixels (Hilbert & Bushouse 2010; Hilbert 2012).

To incorporate information about the appearance of the blobs, the time-dependent blob flags have been combined with one of these two original BPIXTABs to create 25 new BPIXTABs with associated "useafter" dates (Table 2). One of these tables (USEAFTER=2010-06-13) contains the same number of blobs as the prior table

(USEAFTER=2010-04-14) but reflects the second "base" population of bad pixels from w681807ii_bpx.fits. Table 2 lists the useafter date in both ISO standard format and MJD to facilitate comparison to the dates listed in Table 1. Additional *bpx.fits* reference files of the same format will be generated as new blobs are observed, e.g. via the CSM monitoring programs (e.g. program 14020 in Cycle 22).[1]

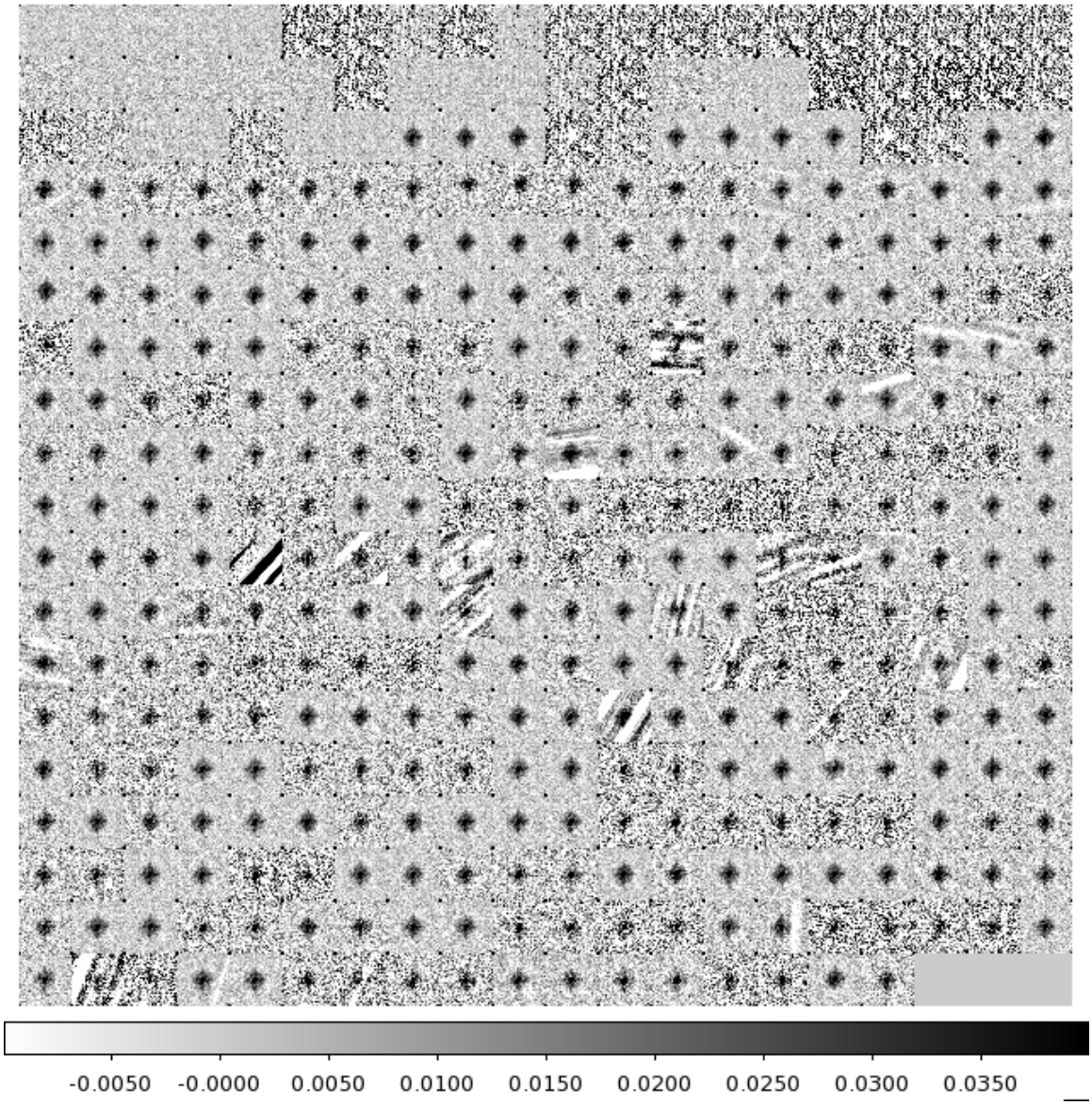


**Figure 2: Grid of Blob #6 at all epochs available from the dark-Earth flat field programs. The grid is organized chronologically, raster scanning from left to right and top to bottom. Blob #6 appears first at MJD 55830.7 (3rd row from top, 8th column from left); the prior image was taken 55754.1. Based upon this, we would flag pixels associated with Blob #6 after MJD 55754.1, except that in this case we have a more accurate date of first arrival from Pirzkal (2012), namely 55806.0, which thus appears**

[1] At press time, more than a year has elapsed since the last new blob has appeared on Jul 30, 2013; we can hope that no more will ever appear.

**also in Table 1 of this work. Saturated images occur occasionally; they show a salt-and-pepper noise pattern and should be ignored.**

## Testing the "useafter" bpx.fits Files

We needed to decide whether to use all 127 blobs listed in Table 1, or perhaps a smaller set, e.g. the union of the 27 strong and 19 medium blobs. Using too many (weak) blobs unnecessarily flags too many pixels. Not flagging enough blobs may allow them to "print through" upon sky background, galaxies, or other extended objects.

There are 27 strong blobs covering 5816 pixels in aggregate, 19 medium blobs covering 3847 pixels, 76 weak blobs covering 8286 pixels, and 5 even-weaker and large-diameter blobs covering 1005 pixels that we added by hand. Note that there are approximately as many pixels in the first two categories (5816+3847 = 9663) as in the last two categories (8286+1005 = 9291). Recall that there are 1 million pixels on the detector, so 9663 pixels corresponds to slightly less than 1% of the detector area.

As an *a priori* case for discussion of the unavoidable compromise of masking too many pixels or too few pixels, we adopt representative parameters of the Frontier Fields program: They observe ~1300-s exposures in a 4-point dither pattern (a 2-point blob dither[2] plus a small 2-point dither to subsample the PSF), as described in Table 3. For the F160W filter, this is repeated twelve times per target field. From the ETC using default values for sky (Zodiacal and Earth shine), we estimate ~1000 e-/pixel for a 1300 sec F160W exposure. Because the observations are repeated twelve times, the effective exposure is ~12,000 e-/pixel at each dither position and ~24,000 e-/pixel at each blob position. For comparison, each of the F153M dark-Earth flats typically has ~10,000 e-/pixel. Since we can see (marginally) each of the faintest blobs in *individual* dark-Earth flats when arrayed as a grid in Figure 2, we expect that a deep astronomical image would also show even the faintest blobs that we have identified if it is exposed to 10,000 e-/pixel in uniform sky. Evidently, because the Frontier Fields exposures have greater than two times more sky at a given blob-dither position, this is a good test set for determining whether the faintest blobs should be included in the masks.

We empirically tested the new "useafter" flags for blobs on Frontier Fields images. We compared two sets of blobs derived from Table 1: A) the union of the 27 strong blobs and the 19 medium blobs, and B) all 127 blobs. Figures 3 and 4 illustrate the differences in the DQ arrays between the nominal BPIXTAB blob flags and those generated under cases A and B, respectively.

[2] The two-point blob dither is ~36 pixels, approximately parallel to the detector's diagonal from the lower left corner to the upper right corner.

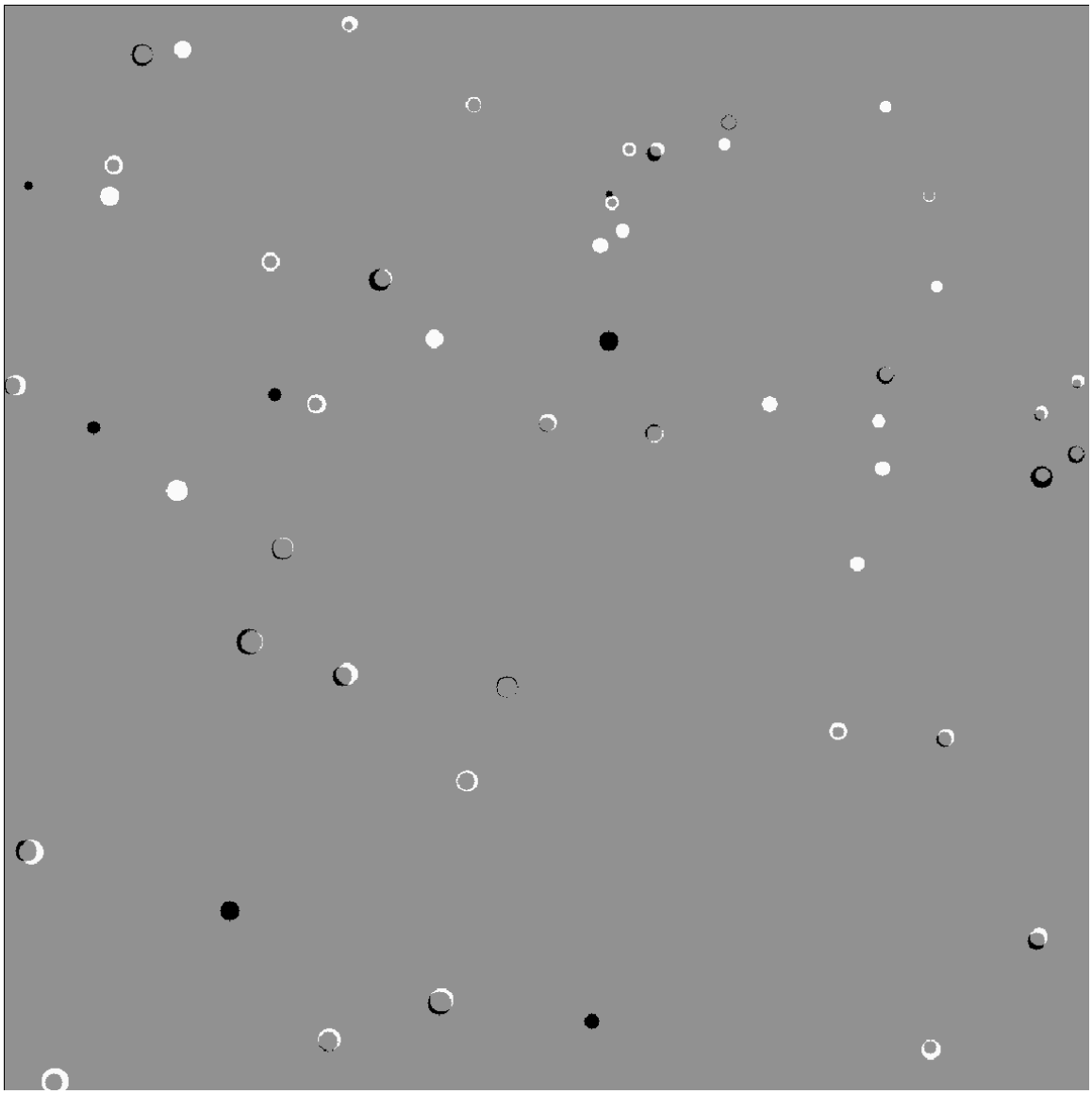

**Figure 3: Difference in the FLT data quality DQ array using the latest blob mask with 46 blobs (27 strong + 19 medium; useafter = Mar 19, 2013) and that in the CALWFC3 pipeline's current bad pixel table (w681807ii_bpx.fits, delivered Apr 26, 2012, useafter = June 13, 2010 ). Positive (white) values show new blobs and negative (black) values show blobs that are no longer flagged in the BPIXTAB (generally "weak" blobs, blue or cyan in Table 1). Crescents or annuli indicate that the blob mask positions and/or radii have been adjusted slightly. We emphasize that once observed in orbit, blobs have never been observed to disappear or to physically move on the detector.**

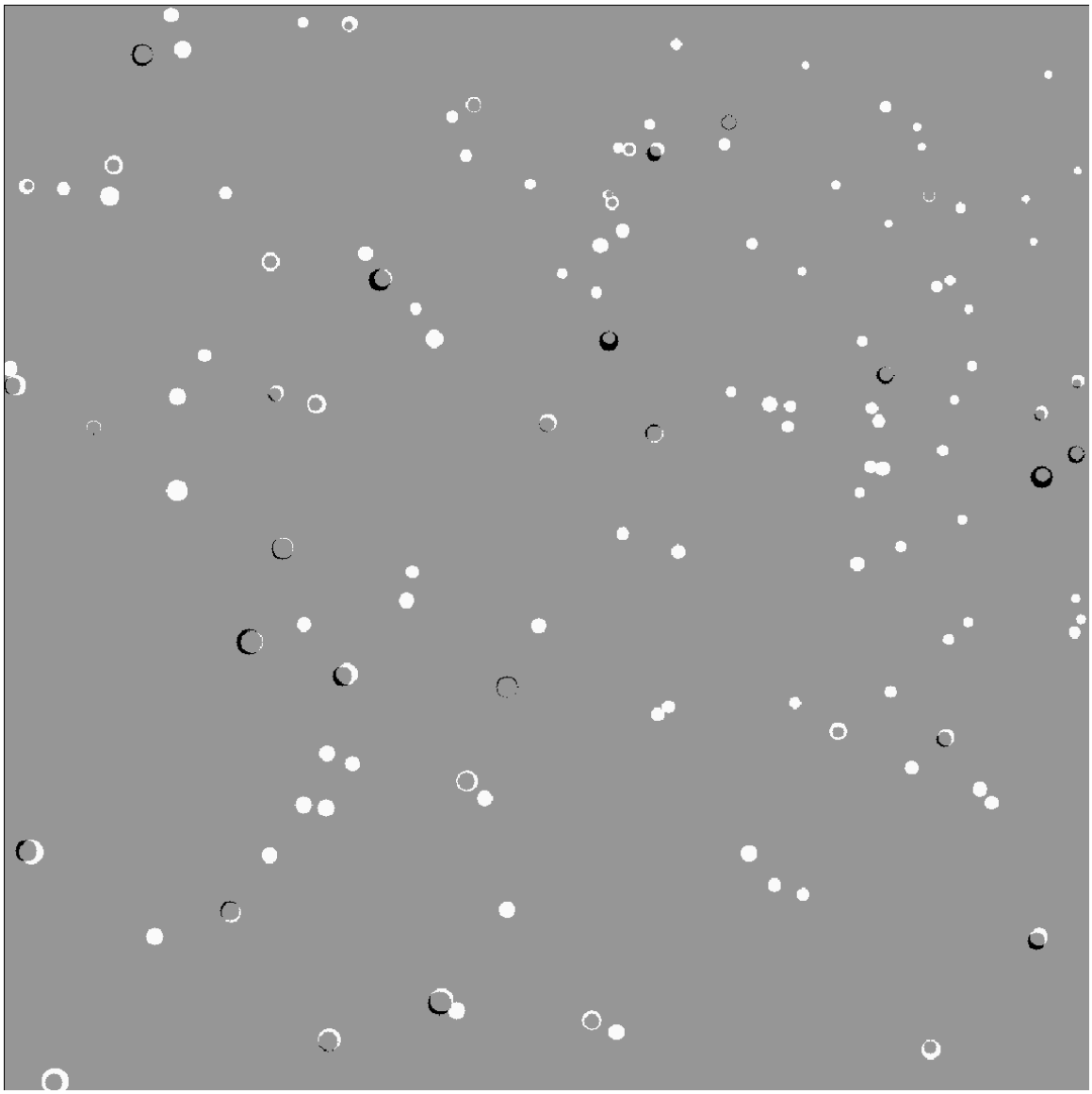

**Figure 4: Same as Figure 3 except here we used all 127 blobs (useafter = Jun 21 2013). Many of the "new" blobs may have been there all along and are only "newly-detected" weak blobs.**

Since the majority of IR programs do not include a blob dither, the default behavior in the OPUS pipeline is to ignore flags of 512 in each image's DQ array when creating drizzled products. This is achieved by setting the AstroDrizzle parameters "driz_sep_bits" and "final_bits" equal to 512 , so that those pixels will be treated as "good" in the final stack. With such analysis, depressions in the calibrated images may occur. Users are encouraged to "blink" the science and DQ arrays in the FLT images to determine if pixels associated with blobs show reduced sensitivity. When combining images taken with a blob dither in AstroDrizzle, users may elect to treat 512 flags as bad pixels, thus removing systematic depressions in the sky caused by the blobs at the cost of reducing the sensitivity within certain pixels of the combined images. To mitigate the

impact of reduced signal-to-noise when blobs are rejected from the stack, observers may wish to define and use a custom 4-point dither pattern that fully steps across the blob in all 4 positions. By doing so, masking blobs will reduce the effective observing time at a given pixel in the final stack by only 25% instead of 50%, by rejecting 1 of 4 positions instead of 1 of 2 positions.

As a test, the MACSJ0416.1-2403 IR parallel field was combined with AstroDrizzle, where pixels flagged as 512 in the BPIXTAB were rejected. Thus, the full stack contained a total sky of ~40,000 electrons in F160W with half the observations at each of the two blob dithers. Two sets of bad pixel tables were tested: 1) one with the 46 strongest blobs (~1% of detector pixels) and 2) a second one with all 127 blobs (~2% of detector pixels). These affect ~2% and ~4% of pixels, respectively, in the final mosaics since the blob dither creates two masked regions for each blob. Figure 5 shows a noticeable improvement in the final mosaics when including the 2 new blobs indicated by the circles. While we expected to find that including the blob masks in the stack reduced the r.m.s. of the background, to the contrary it results in a larger total r.m.s. for those pixels, because masking the blobs decreases by a factor of two the effective observing time of the image in those pixels. Evidently in this case, the attenuation of the blobs is small compared to the effect of excluding half the observing time for those pixels. However, including the masks removes depressions in the sky background (Figure 5) and therefore should remove systematic effects in extended-source photometry. For example, a galaxy falling on a blob in half the exposures will no longer be impacted by the spatially dependent response caused by the blob. While the new set of 46 blobs visibly improved the quality of the mosaics, the full set of 127 did not, and resulted in slightly increased noise in the final image. As before with the stronger blobs, this is because the attenuation of the weak blobs is much smaller than the effect of reducing the signal-to-noise by $\sqrt{2}$. Moreover, including 127 blobs (2% of the detector pixels) at 2 dither positions reduces the total depth in ~4% of pixels in final image, so we elected to not mask those pixels in the final mosaics. Based upon this case study, we include only the strong and medium blobs in the BPIXTAB, i.e. the red and green respectively in Table 1 and Figure 1.

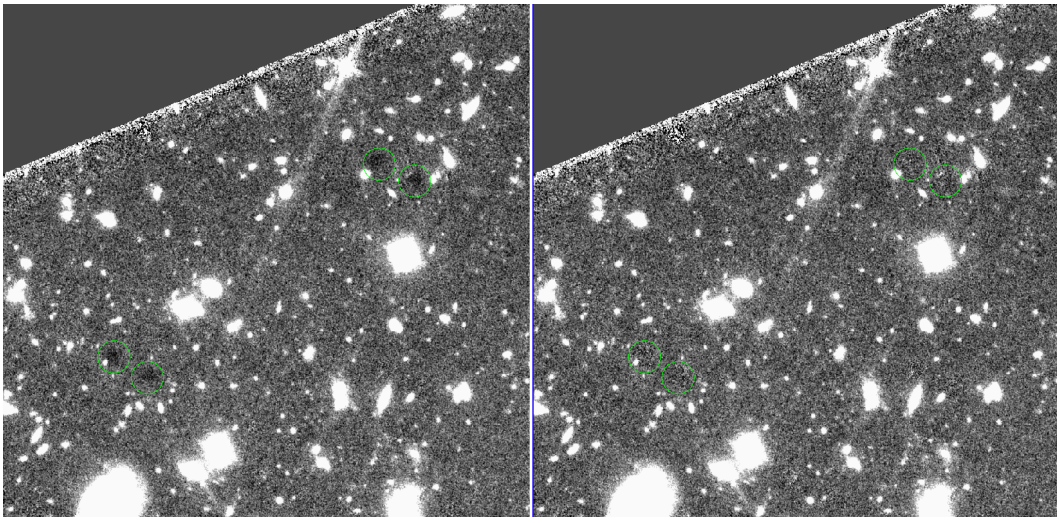

**Figure 5: Comparison using the original BPIXTAB (w681807ii_bpx.fits) versus the newer 46 blob BPIXTAB derived in this work (useafter=Mar 19 2013). Two pairs of strong blobs that were not masked in the original mosaic (left) have been corrected in the new mosaics (right), resulting in a more uniform sky background. When sources fall on pixels affected by blobs, removing systematics in the image response is important for accurate photometry and morphology. Mosaics of the MACSJ0416.1-2403 parallel field in F160W from Frontier Fields (Lotz et al. 2014) are shown.**

## Application of a Blob Flat Field

In all of what has been described heretofore in this report, we treat the pixels affected by blobs as uncorrectable and requiring flagging: i.e. the strategy is to work around the blobs by dithering. In this section and Figure 6 we show that we can correct the pixels affected by the blobs using an appropriate flat field. We made a "blob flat field" that is unity everywhere except inside each blob's radius, where we replace unity with the average of a large number of F153M ima.fits images of the dark Earth. By using extension 1 of the F153M ima.fits images, we obtain the dark subtraction, nonlinearity correction, and flat fielding nominally applied by the CALWF3 pipeline. Because that nominal processing is applied both to each science image and to each of the F153M images of the dark Earth, the average of the latter images, each renormalized to a median value of unity, should provide a flat field appropriate for correcting the science images. Generally, ~1/3 of images in the dark-Earth program are affected by trails across the images caused by city lights. Hence, in creating the average image, we did not include any image with an r.m.s. inconsistent with Poisson noise combined in quadrature with a 0.45% r.m.s. spatial variation (fixed pattern noise) across the image.

Figure 6 illustrates a science image exhibiting bright, extended nebulosity; the blobs essentially disappear after division by the blob flat field. Application of such a blob flat field could be especially helpful in cases where dithered images are not available, and the goal is to improve the image's cosmetic appearance. It may also improve photometry of

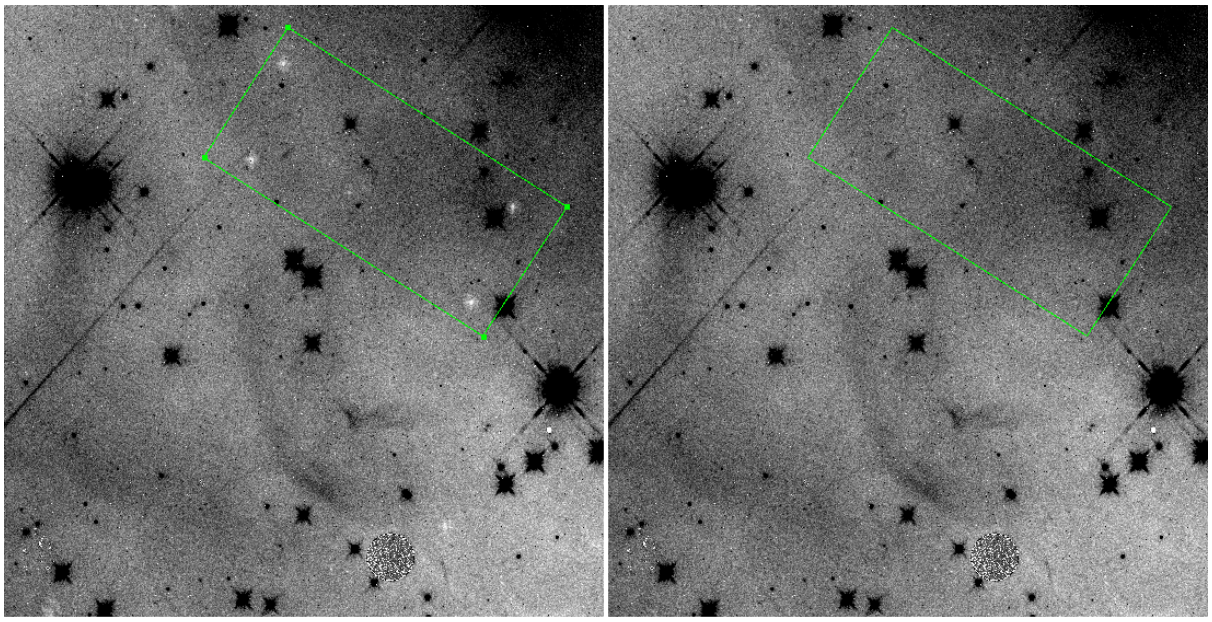

**Figure 6: (Left) Original image showing at least 6 prominent blobs as fainter areas in the nebulosity of NGC 2174. Four blobs are enclosed by the tilted rectangle. We display only the lower left quadrant of the image (Program 13623's ichx04jyq_flt.fits, a 1103-s, F105W exposure. (Right) Same area of the image, after correction by division by the blob flat field. Although such division improves images' cosmetic appearance and it may improve photometry of extended sources, we expect that it can create systematic errors for stellar photometry (see text).**

extended sources such as nebulae and galaxies. For the blob flat field we used all 127 blobs, because we expect each blob to have its appropriate effect on the data. Only "strong" blobs show a noticeable effect in the example that we examined. We note also that because 98% of the pixels are exactly unity, for those pixels specifically, application of the blob flat field will "do no harm," just like the doctor's creed.

*However*, we warn the reader that we expect that application of a blob flat field will create (not correct) errors for stellar photometry. The reason is that the particulates responsible for the blobs are very small, with optical cross sections comparable to, or more typically smaller than, the size of a single IR pixel. Even for a star whose image lies within a blob on the detector, the "footprint" of its beam of light on the CSM typically will miss the particulate entirely, and hence it's photometry will be unaffected by the particulate. Consequently, dividing by the blob flat field would erroneously increase the star's photometric value. For the complicated case of stellar photometry in the presence of bright, extended emission, we recommend the traditional approach of flagging and dithering rather than flat fielding the blobs.

Extending earlier work comparing the effective scattering cross sections of blobs in filters F105W, F125W, and F160W (Pirzkal & Hilbert 2012; Pirzkal, Viana, & Rajan 2010), we find a slight but noticeable wavelength dependence for each blob's shape. For filters F098M, F105W, F110W, F125W, and F127M, the radial profile of each dark-Earth flat's difference from that for F153M changes from negative in the blob cores, to

positive, and back to negative before asymptotically returning to zero far from each blob's center. The differences are noticeable in high signal to noise images such as dark-Earth flat fields, but they are not noticeable in Figure 6, a F105W example. For filters F139M, F140W, and F160W, their blobs' profiles are almost indistinguishable from F153M's.

In all cases, mis-registration of the blobs caused by changes in the CSM position from visit to visit can be much larger than any wavelength dependence. Because of that, we made seven separate blob flat fields, each one generated from a distinct set of F153M images corresponding to seven slightly different positions of the CSM, spanning ~1 pixel of shift on the detector.[3] A future report will examine flat fielding of blobs more thoroughly and quantitatively.

Of course, one should not use both the blob flat field and the blob flags in the BPIXTAB, because the latter will force the pipeline to ignore the pixels inside the blobs, making moot the blob flat field. However, the BPIXTAB's useafter dates may be required to revise the blob flat field, i.e. to replace with unity those specific pixel values for blobs that did not exist at the time the science observations were made.

## Conclusions

A total of 127 blobs, defocused images of particulates on the channel select mechanism, have been identified on WFC3 imagery (Table 1 and Figure 1). Appropriate "useafter" keywords for the 27 "strong" and 19 "medium" strength new blobs (46 total) have been implemented in the CALWFC3 pipeline as BPIXTABs in CRDS (Table 2). We discuss the compromise between including or excluding "weak" blobs in the BPIXTAB tables; we chose to exclude them. When a new blob is detected in the future, it can be added to the list of blobs and a new BPIXTAB table can be issued. Alternatively, instead of flagging pixels affected by blobs, a user can apply a custom-made "delta" flat field derived from many F153M dark-Earth flat fields, exclusively for pixels within the blobs, and unity elsewhere. Application of such a flat field improves the cosmetic appearance of the image (Figure 6) but is expected to create (not correct) photometric errors for stars.

One of us (B. Hilbert) wrote scripts to convert a list of blobs such as Table 1 into files in BPIXTAB format; the curator of those scripts hereafter is Ben Sunnquist. The authors thank Tom Wheeler, John MacKenty, and Nor Pirzkal, for discussions and assistance. We thank Elena Sabbi for comments that improved the manuscript.

[3] Blob flat fields will be distributed via the WFC3 website.

## References

Bushouse, H 2005, CSM Particulate Investigation, ISR WFC3 2005-26.

Bushouse, H. & Kalirai, J. 2008, CSM Mapping of the UVIS Field of View, ISR WFC3 2008-45.

Fienberg, D. 2009, WFC3 Systems Description and Users Handbook.

Hilbert, B. & Bushouse, H. 2010, WFC3/IR Bad Pixel Table: Update Using Cycle 17 Data, WFC3 ISR 2010-13

Hilbert, B. 2012, WFC3/IR Cycle 19 Bad Pixel Table Update, WFC3 ISR 2012-10

Koekemoer, A. et al. 2014, The HST Frontier Fields: Science Data Pipeline, Products, and First Data Release, 2014AAS...22325402K

Lotz, J. et al. 2014, The HST Frontier Fields, 2014AAS...22325401L

Pirzkal, N., Viana, A., & Rajan, A. 2010, The WFC3 IR "Blobs," ISR WFC3 2010-06.

Pirzkal, N. & Hilbert, B. 2012, The WFC3 IR "Blobs" Monitoring, ISR WFC3 2012-15

## Revisions

Blobs discovered after the original publication of this report have been recorded in Table 4. Of these new blobs, #134, #137, #140, #141, #142 and #145 have warranted inclusion in an updated BPIXTAB (Table 5). Their inclusion was justified after measuring the sum of pixel values within a circular aperture centered on the blob and confirming that this value was consistent with those of currently masked (i.e. red and green) blobs.

Table 1: List of Blobs

| Index | X | Y | Radius | Color | Flux | First Appearance (MJD) |
|---|---|---|---|---|---|---|
| 1 | 102.9 | 839.3 | 9.0 | color=red | 62.7 | 56370.3633 |
| 2 | 106.9 | 868.2 | 8.9 | color=red | 55.3 | 55043 |
| 3 | 134.1 | 971.5 | 8.3 | color=red | 181.4 | 55187.5 |
| 4 | 171.3 | 976.3 | 8.1 | color=red | 52.9 | 55043.0 |
| 5 | 235.8 | 423.1 | 10.2 | color=red | 159.7 | 55383.5 |
| 6 | 253.0 | 778.0 | 8.6 | color=red | 78.8 | 55806. |
| 7 | 264.9 | 511.1 | 9.7 | color=red | 78.0 | 55754.0664 |
| 8 | 296.1 | 645.2 | 9.0 | color=red | 100.3 | 55898.2969 |
| 9 | 324.6 | 393.4 | 10.0 | color=red | 62.5 | 55043 |
| 10 | 326.9 | 1000.1 | 7.4 | color=red | 54.0 | 55150 |
| 11 | 358.1 | 762.8 | 8.2 | color=red | 130.3 | 55042.99 |
| 12 | 413.0 | 89.0 | 10.9 | color=red | 53.8 | 55100 |
| 13 | 436.7 | 293.2 | 9.9 | color=red | 83.4 | 55863 |
| 14 | 442.8 | 924.7 | 7.2 | color=red | 85.0 | 55250 |
| 15 | 474.3 | 380.4 | 9.4 | color=red | 179.5 | 55175 |
| 16 | 512.2 | 627.8 | 8.2 | color=red | 57.1 | 55800 |
| 17 | 588.1 | 883.1 | 6.8 | color=red | 55.1 | 55043 |
| 18 | 611.8 | 617.2 | 7.8 | color=red | 112.9 | 55059 |
| 19 | 614.0 | 883.2 | 6.6 | color=red | 79.6 | 55043 |
| 20 | 681.1 | 908.2 | 6.3 | color=red | 83.9 | 55150 |
| 21 | 719.0 | 645.0 | 7.2 | color=red | 55.3 | 55043.0 |
| 22 | 783.0 | 339.7 | 8.2 | color=red | 78.9 | 55800 |
| 23 | 827.9 | 673.2 | 6.6 | color=red | 100.3 | 55043 |
| 24 | 868.0 | 839.2 | 5.8 | color=red | 60.2 | 55043 |
| 25 | 884.1 | 334.2 | 7.8 | color=red | 83.4 | 55043 |
| 26 | 970.6 | 147.8 | 8.3 | color=red | 130.3 | 55125 |
| 27 | 974.0 | 579.1 | 6.4 | color=red | 92.7 | 55043 |
| 28 | 15.3 | 662.7 | 9.7 | color=green | 29.3 | 55811.9 |
| 29 | 30.0 | 227.0 | 11.3 | color=green | 29.0 | 55043 |
| 30 | 52.0 | 13.0 | 12.7 | color=green | 50.0 | 55071 |
| 31 | 165.8 | 564.3 | 9.9 | color=green | 36.1 | 56327.2852 |
| 32 | 308.0 | 52.0 | 10.4 | color=green | 26.4 | 55038.5 |
| 33 | 406.0 | 706.0 | 8.3 | color=green | 37.8 | 55043.0 |
| 34 | 561.1 | 793.2 | 7.3 | color=green | 32.7 | 55402.7 |
| 35 | 571.7 | 833.2 | 6.7 | color=green | 29.2 | 55300 |
| 36 | 582.1 | 807.0 | 6.5 | color=green | 27.1 | 55402.7 |
| 37 | 676.9 | 887.4 | 5.8 | color=green | 26.9 | 55898.2969 |
| 38 | 800.9 | 496.0 | 6.9 | color=green | 26.9 | 55402.7 |
| 39 | 821.0 | 629.2 | 6.2 | color=green | 26.4 | 55402.7 |
| 40 | 824.6 | 584.9 | 7.0 | color=green | 31.9 | 55402.7 |
| 41 | 827.3 | 922.8 | 5.6 | color=green | 38.3 | 55043.0 |
| 42 | 869.6 | 42.7 | 9.1 | color=green | 36.1 | 55043 |
| 43 | 874.9 | 755.1 | 5.6 | color=green | 27.6 | 55402.7 |
| 44 | 973.0 | 637.0 | 6.2 | color=green | 51.2 | 55043 |
| 45 | 1006.0 | 599.0 | 6.2 | color=green | 52.3 | 55088.8 |
| 46 | 1007.0 | 667.0 | 5.9 | color=green | 42.4 | 55796.7 |
| 47 | 9.7 | 678.3 | 7.2 | color=blue | 16.2 | 55402.7 |
| 48 | 25.4 | 848.4 | 7.1 | color=blue | 18.8 | 55200 |
| 49 | 59.8 | 846.3 | 6.3 | color=blue | 15.2 | 55402.7 |
| 50 | 88.3 | 623.5 | 6.5 | color=blue | 13.6 | 55374 |
| 51 | 160.3 | 1008.1 | 7.1 | color=blue | 24.9 | 55043.0 |
| 52 | 191.5 | 690.8 | 6.2 | color=blue | 14.4 | 55898.3 |
| 53 | 211.0 | 842.3 | 6.1 | color=blue | 16.4 | 55402.7 |
| 54 | 216.4 | 170.7 | 9.0 | color=blue | 14.9 | 55841.3 |
| 55 | 252.2 | 223.9 | 7.7 | color=blue | 15.6 | 56082 |
| 56 | 258.7 | 655.6 | 7.0 | color=blue | 18.7 | 55402.7 |
| 57 | 283.2 | 1001.3 | 5.1 | color=blue | 14.6 | 55402.7 |
| 58 | 284.4 | 439.4 | 6.9 | color=blue | 15.3 | 55402.7 |
| 59 | 306.0 | 319.0 | 7.5 | color=blue | 16.7 | 55043.0 |
| 60 | 329.7 | 309.3 | 6.8 | color=blue | 14.0 | 55754.1 |
| 61 | 341.8 | 785.7 | 7.2 | color=blue | 24.3 | 55402.7 |
| 62 | 380.1 | 461.7 | 7.4 | color=blue | 19.7 | 55402.7 |
| 63 | 385.6 | 488.3 | 6.0 | color=blue | 13.4 | 55402.7 |
| 64 | 388.6 | 734.3 | 5.6 | color=blue | 14.7 | 55402.7 |
| 65 | 422.9 | 913.4 | 5.8 | color=blue | 20.1 | 55402.7 |
| 66 | 435.5 | 877.1 | 5.8 | color=blue | 19.6 | 55402.7 |
| 67 | 453.1 | 277.2 | 7.3 | color=blue | 17.4 | 55402.7 |

```
 68 circle( 474.0, 173.2,   7.6) # color=blue    17.6  55043.0
 69 circle( 495.4, 850.6,   5.0) # color=blue    15.3  55402.7
 70 circle( 503.3, 438.1,   7.0) # color=blue    19.4  55402.7
 71 circle( 525.6, 766.8,   5.0) # color=blue    14.3  55402.7
 72 circle( 553.0,  70.0,   9.2) # color=blue    25.3  55811.9
 73 circle( 557.5, 749.3,   5.4) # color=blue    17.1  55402.7
 74 circle( 568.0, 840.5,   4.6) # color=blue    13.7  55042.99
 75 circle( 569.2, 707.0,   5.4) # color=blue    16.1  55043.
 76 circle( 576.0,  59.0,   7.7) # color=blue    18.1  56464.89
 77 circle( 577.5, 884.6,   5.1) # color=blue    17.8  55402.7
 78 circle( 582.1, 524.1,   6.0) # color=blue    16.6  56464.89
 79 circle( 607.3, 906.2,   5.2) # color=blue    19.7  55402.7
 80 circle( 614.7, 355.6,   6.3) # color=blue    16.2  55402.7
 81 circle( 624.6, 362.9,   6.1) # color=blue    15.3  55402.7
 82 circle( 632.0, 980.9,   5.2) # color=blue    23.1  55402.7
 83 circle( 633.8, 507.4,   6.7) # color=blue    21.4  55402.7
 84 circle( 682.9, 656.5,   5.0) # color=blue    15.2  55402.7
 85 circle( 699.8, 225.7,   8.2) # color=blue    26.1  55043.0
 86 circle( 702.8, 795.0,   5.5) # color=blue    21.8  55402.7
 87 circle( 723.5, 196.4,   6.5) # color=blue    16.3  55402.7
 88 circle( 736.0, 623.8,   5.6) # color=blue    19.4  55402.7
 89 circle( 738.3, 643.2,   5.6) # color=blue    19.9  55402.7
 90 circle( 742.7, 366.1,   5.5) # color=blue    13.9  55996.2
 91 circle( 749.3, 769.0,   4.2) # color=blue    13.1  55402.7
 92 circle( 750.3, 187.3,   6.0) # color=blue    14.0  55402.7
 93 circle( 752.6, 961.4,   3.7) # color=blue    13.3  55402.7
 94 circle( 781.0, 849.7,   4.3) # color=blue    15.7  55402.7
 95 circle( 803.0, 562.7,   5.0) # color=blue    15.4  55402.7
 96 circle( 805.8, 703.8,   5.2) # color=blue    19.6  55402.7
 97 circle( 813.4, 586.8,   6.1) # color=blue    23.8  55402.7
 98 circle( 814.4, 641.3,   5.8) # color=blue    22.7  55402.7
 99 circle( 830.2, 813.6,   3.9) # color=blue    13.7  55402.7
100 circle( 832.0, 376.5,   5.5) # color=blue    15.5  55402.7
101 circle( 841.3, 511.9,   5.4) # color=blue    17.8  55402.7
102 circle( 851.6, 305.7,   6.7) # color=blue    22.0  55402.7
103 circle( 856.3, 903.6,   4.0) # color=blue    17.0  55402.7
104 circle( 861.1, 885.4,   4.0) # color=blue    16.1  55402.7
105 circle( 880.7, 601.8,   5.3) # color=blue    20.3  55402.7
106 circle( 886.2, 425.4,   5.4) # color=blue    16.7  55402.7
107 circle( 887.4, 760.6,   4.9) # color=blue    21.5  56082
108 circle( 891.6, 649.0,   4.5) # color=blue    15.6  55402.7
109 circle( 897.0, 828.2,   5.0) # color=blue    25.1  55402.7
110 circle( 898.7, 537.2,   4.7) # color=blue    14.6  55402.7
111 circle( 904.0, 441.5,   4.8) # color=blue    14.0  55402.7
112 circle( 904.6, 733.6,   4.3) # color=blue    16.1  56246.8
113 circle( 908.0, 680.6,   4.9) # color=blue    19.6  55402.7
114 circle( 915.3, 285.7,   6.9) # color=blue    24.1  55402.7
115 circle( 926.2, 272.9,   6.5) # color=blue    21.3  55402.7
116 circle( 958.3, 836.7,   3.8) # color=blue    16.2  55402.7
117 circle( 965.7, 796.9,   3.7) # color=blue    16.0  55402.7
118 circle( 979.3, 952.6,   3.7) # color=blue    18.6  55402.7
119 circle(1003.7, 432.1,   5.6) # color=blue    20.8  55402.7
120 circle(1004.8, 463.4,   4.3) # color=blue    13.1  55402.7
121 circle(1006.9, 862.9,   3.7) # color=blue    17.3  55402.7
122 circle(1009.5, 444.5,   4.7) # color=blue    14.9  55402.7
123 circle( 145.0, 148.0,   8.0) # color=cyan   <13.1  55402.7
124 circle( 305.0, 268.0,   8.0) # color=cyan   <13.1  55402.7
125 circle( 427.0,  79.0,   8.0) # color=cyan   <13.1  55402.7
126 circle( 284.0, 271.0,   8.0) # color=cyan   <13.1  55402.7
127 circle( 166.0, 652.0,   8.0) # color=cyan   <13.1  55402.7
```

Notes: Only the strongest 46 blobs (red and green colors) are included in the published BPIXTAB bad pixel tables. By trimming away the first and last columns, e.g. by awk '{print substr($0,5,43)}', the table can be appended to a ds9 reg file for convenient display. See Table 4 for any updates to Table 1. **The 'First Appearance' date in this Table corresponds to the last date the blob *wasn't* seen in the dark-Earth monitoring images; this ensures that the blob will be flagged in all science images in which the blob could appear.**

Table 2: Time-dependent bad pixel tables, with 25 unique 'useafter' dates.

Source: BPIXTAB retrieved on Jul 1, 2014 from https://hst-crds.stsci.edu/
The new BPIXTAB files described in this ISR begin with the letter “y” below.

| USEAFTER | BPIXTAB | USEAFTER(MJD) |
|---|---|---|
| 1991-01-01 00:00:00 | q911321ki_bpx.fits | 48257.000 |
| 2008-02-20 00:00:00 | t291659ni_bpx.fits | 54516.000 |
| 2009-05-14 00:00:00 | u4c1709ri_bpx.fits | 54965.000 |
| 2009-07-26 12:00:00 | y711519ji_bpx.fits | 55038.500 |
| 2009-07-30 23:45:36 | y711519ki_bpx.fits | 55042.990 |
| 2009-07-31 00:00:00 | y711519li_bpx.fits | 55043.000 |
| 2009-08-16 00:00:00 | y711519mi_bpx.fits | 55059.000 |
| 2009-08-28 00:00:00 | y711519ni_bpx.fits | 55071.000 |
| 2009-09-14 19:12:00 | y711519oi_bpx.fits | 55088.800 |
| 2009-09-26 00:00:00 | y711519pi_bpx.fits | 55100.000 |
| 2009-10-21 00:00:00 | y711519qi_bpx.fits | 55125.000 |
| 2009-11-15 00:00:00 | y711519ri_bpx.fits | 55150.000 |
| 2009-12-10 00:00:00 | y711519si_bpx.fits | 55175.000 |
| 2009-12-22 12:00:00 | y711519ti_bpx.fits | 55187.500 |
| 2010-02-23 00:00:00 | y7115200i_bpx.fits | 55250.000 |
| 2010-04-14 00:00:00 | y7115201i_bpx.fits | 55300.000 |
| 2010-06-13 00:00:00 | y7115202i_bpx.fits | 55360.000 |
| 2010-07-06 12:00:00 | y7115203i_bpx.fits | 55383.500 |
| 2010-07-25 16:48:00 | y7115204i_bpx.fits | 55402.700 |
| 2011-07-12 01:35:36 | y7115205i_bpx.fits | 55754.066 |
| 2011-08-23 16:48:00 | y7115206i_bpx.fits | 55796.700 |
| 2011-08-27 00:00:00 | y7115207i_bpx.fits | 55800.000 |
| 2011-09-02 00:00:00 | y7115208i_bpx.fits | 55806.000 |
| 2011-09-07 21:36:00 | y7115209i_bpx.fits | 55811.900 |
| 2011-10-29 00:00:00 | y711520ai_bpx.fits | 55863.000 |
| 2011-12-03 07:07:32 | y711520bi_bpx.fits | 55898.297 |
| 2013-02-04 06:50:41 | y711520ci_bpx.fits | 56327.285 |
| 2013-03-19 08:43:09 | y711520di_bpx.fits | 56370.363 |

Note: As justified in the text, these files exclude the 81 “weak” blobs, colored blue or cyan in Figure 1 and Table 1. The last file listed contains 46 blobs. See Table 5 for any updates to Table 2.

Table 3: Typical Frontier Fields dither pattern for a single visit.

| Image Name | X-dither (") | Y-dither (") | X-dither (pix) | Y-dither (pix) |
|---|---|---|---|---|
| ic8o01iqq_raw.fits | -1.948458 | -2.280334 | -15.19 | -17.77 |
| ic8o01isq_raw.fits | -2.151460 | -1.977332 | -16.77 | -15.41 |
| ic8o01iwq_raw.fits | 1.371545 | 0.989666 | 10.69 | 7.71 |
| ic8o01izq_raw.fits | 1.168543 | 1.292668 | 9.11 | 10.08 |

Table 4: List of Blobs; Updates since original report

| Index | X | Y | Radius | Color | Flux | First Appearance (MJD) |
|---|---|---|---|---|---|---|
| 128 | circle( 87.0, | 414.0, | 8.0) # | color=cyan | n/a | 57196.9504 |
| 129 | circle( 279.0, | 602.0, | 7.0) # | color=blue | 16 | 57379.4345 |
| 130 | circle( 276.0, | 583.0, | 7.0) # | color=cyan | n/a | 57664.1565 |
| 131 | circle( 495.0, | 528.0, | 8.0) # | color=blue | n/a | 57693.5125 |
| 132 | circle( 340.0, | 398.0, | 7.2) # | color=cyan | 17 | 56530.1606 |
| 133 | circle( 962.0, | 494.0, | 6.7) # | color=blue | 26 | 57857.4647 |
| 134 | circle( 969.0, | 476.0, | 7.5) # | color=red | 95 | 57939.3281 |
| 135 | circle( 853.0, | 283.0, | 8.0) # | color=blue | 26 | 57942.2520 |
| 136 | circle( 434.0, | 770.0, | 4.9) # | color=cyan | 13 | 57962.8495 |
| 137 | circle( 566.0, | 874.0, | 6.9) # | color=green | 35 | 57978.4207 |
| 138 | circle( 737.0, | 952.0, | 5.2) # | color=blue | 25 | 58045.9132 |
| 139 | circle( 438.0, | 643.0, | 6.7) # | color=blue | 20 | 58062.4709 |
| 140 | circle( 853.0, | 711.0, | 9.0) # | color=red | 180 | 58062.4709 |
| 141 | circle( 695.0, | 520.0, | 8.0) # | color=red | 95 | 58073.5360 |
| 142 | circle( 352.0, | 122.0, | 10.0) # | color=green | 26.3 | 58106.1018 |
| 143 | circle( 955.0, | 360.0, | 6.4) # | color=blue | 24 | 58121.2071 |
| 144 | circle( 404.0, | 801.0, | 6.1) # | color=blue | 19 | 58174.1477 |
| 145 | circle( 268.0, | 613.0, | 9.0) # | color=green | 30 | 58174.1477 |
| 146 | circle( 736.0, | 151.0, | 6.3) # | color=blue | 15 | 58188.3145 |

Note: Nothing in this report has been updated besides Tables 4 and 5; in particular, the figures remain as they were originally. Fluxes and radii of this Table may be less accurate than for those of Table 1, because for expediency, fluxes are estimated here by visual comparison with other blobs in Table 1. Of these new blobs, #134, #137, #140, #141, #142 and #145 have warranted the creation of an updated BPIXTAB (Table 5). **The 'First Appearance' date in this Table corresponds to the last date the blob *wasn't* seen in the dark-Earth monitoring images; this ensures that the blob will be flagged in all science images in which the blob could appear.**

Table 5: Time-dependent bad pixel tables; Updates since original report

| USEAFTER | BPIXTAB | USEAFTER(MJD) |
|---|---|---|
| 2017-07-05 07:52:27 | 17i18351i_bpx.fits | 57939.328 |
| 2017-08-13 10:05:48 | 18o1424pi_bpx.fits | 57978.421 |
| 2017-11-05 11:18:09 | 1be19183i_bpx.fits | 58062.471 |
| 2017-11-16 12:51:54 | 1c41413ti_bpx.fits | 58073.536 |
| 2017-12-19 02:26:37 | 21820228i_bpx.fits | 58106.102 |
| 2018-02-25 03:32:40 | 2361319pi_bpx.fits | 58174.148 |

Note: Nothing in this report has been updated besides Tables 4 and 5; in particular, the figures remain as they were originally.